2D-Measurement of Penning Ionization Cross Section upon Molecular Orientation and Collision Energy in $Ar(^3P_{2,0})$ + $CHCl_3$ Crossed Beam Reaction

Masanori Yamato,[†] Hiroshi Ohoyama,*[,†] and Toshio Kasai*[,†,‡]

Department of Chemistry, Graduate School of Science, Osaka University, Toyonaka, Osaka 560-0043, Japan, and Institute for Molecular Science, 38 Nishigonaka, Myodaiji, Okazaki 444-8585, Japan

Received: June 7, 2000; In Final Form: January 9, 2001

The Penning ionization cross section of Ar* + $CHCl_3$ crossed beam reaction is determined as the function of both molecular orientation and relative collision energy using oriented $CHCl_3$ molecular beam and TOF measurement. We find that the steric opacity function at low collision energies is well correlated to the exterior electron density distribution of the $CHCl_3$ molecular orbital that plays a key role in the electron exchange. At high collision energies, however, the reactivity along the molecular axis becomes favorable while the sideways approach on the other hand becomes unfavorable. The result of our ab initio calculation reveals that this collision energy dependence of the sideways approach shows clear discrepancy with the generally accepted propensity rule for repulsive interaction potential. We propose here that this discrepancy can be ascribed to the dependent competition of product branching between Penning ionization and that neutral dissociation varies as collision energy.

I. Introduction

Penning ionization is one of the major processes for de-excitation of metastable atoms by collisions with molecules. $A^* + B \rightarrow A + B^+ + e^-$ is a typical scheme for this reaction, where A* means a metastable atom that should have excitation energy higher than the ionization potential of B. It has been recognized that collision energy and the angle of attack play important roles in Penning ionization. This perspective is based on the proposal originally made by Hotop and Niehaus in 1969. They claim that the ionization takes place via the electron exchange mainly at the turning point; namely, transfer of an outer-shell electron of a target molecule into an inner-shell vacancy of an excited rare-gas atom, which in turn ejects the external electron.[1] That is, the ionization probability is ruled by the extent of mutual overlap between atomic and molecular orbitals involved.

The overall stereoanisotropic effect in Penning ionization is attributed to the sum effect of anisotropy of interaction potential between the colliding pair, and also anisotropy of electron density distribution of relevant molecular orbital. Since we can assign the Penning electron at a fixed enenrgy to a specific molecular orbital which exhibits characteristic spatial distribution of the exterior electron,[2,3] collision energy dependence measurement of the ionization cross section on each specific Penning electron has been applied to elucidate stereoanisotropy of the individual molecular orbital.[2−8] In such studies, the same result on collision energy dependence of partial cross sections is commonly employed to interpret interaction potential as well. Therefore, it is quite tempting to perform an experiment on collision energy dependence under orientation angle-specified conditions. We present here a new type of 2D measurement, where we combine a time-of-flight technique for velocity analysis and a technique of electrostatic hexapole state selection for orientation confinement. Utilizing this method, we clarify the role of collision energy and molecular orientation separately for understanding stereodynamical aspects of Penning ionization by active control of molecular orientations for the $Ar(^3P_{2,0})$ + $CHCl_3 \rightarrow Ar + CHCl_2^+ + Cl + e^-$ reaction in the 0.08−0.18 eV collision energy range, where it had been reported that $CHCl_2^+$ is the only ion product.[9]

II. Experimental Section

Figure 1 shows the experimental setup employed in this work, which has been described more fully elsewhere,[10] thus only a brief description is given with reference to the Newton diagram for the $Ar(^3P_{2,0})$ + $CHCl_3$ colliding system.

To carry out the velocity-resolved analysis, the velocity distributions of the metastable atoms $Ar(^3P_{2,0})$, or Ar* in brief, and the product ion $CHCl_2^+$ are determined by a conventional time-of-flight (TOF) technique with the flight length of 350 mm. The Ar* beam with 35 μs pulse width is generated by the pulsed glow discharge between grid and filament.[11] The glow discharge was ignited by the pulsed grid voltage, which provides the time origin for the TOF measurement. The TOF profile of Ar* was directly measured by a secondary electron multiplier (SEM) mounted on the positive electrode of the orienting field at the beam crossing point. Ar* metastable atom has two fine-states with different energies: $^3P_0$(11.723 eV) and $^3P_2$(11.548 eV). Since the $^3P_0$ state has a higher energy by 0.175 eV than the $^3P_2$ state, the collision energy dependence of the cross section is expected to be shifted by this amount. The relative population of $^3P_0$ to $^3P_2$, i.e., $^3P_0/^3P_2$, had been determined to be 0.02 for our beam source.[12] From this result, the contribution from $^3P_0$ is expected to be negligibly small. In other word, it is a good assumption that the present result can be attributed to the reaction from the $^3P_2$ state.

The pulsed $CHCl_3$ beam with 10 ms width is rotationally state-selected in the 60 cm long electrostatic hexapole field. The state-selected $CHCl_3$ molecules are then oriented in a homogeneous electric field of 1.5 kV/cm strength and then cross the

[†] Osaka University.
[‡] Institute for Molecular Science.

10.1021/jp0020687 CCC: $20.00
Published on Web 03/08/2001

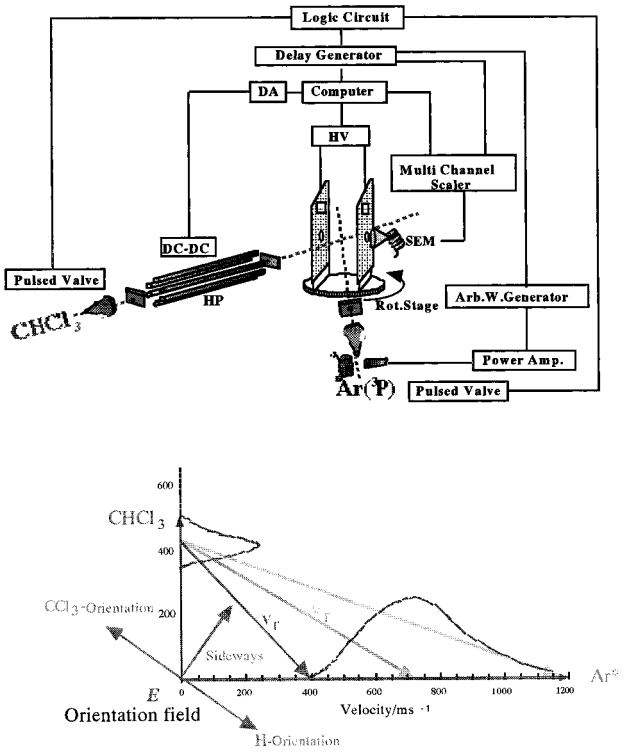

Figure 1. Experimental setup with a Newton diagram. Three molecular orientations, the CCl_3-end, the H-end, and the sideways, are achieved by fixing the homogeneous orientation field with respect to the relative velocity.

pulsed Ar* beam with 35 μs width at a right angle in the same homogeneous field. The orienting homogeneous field is rotatable to choose three different molecular orientations, namely the CCl_3-end, the H-end, and the sideways, with respect to the relative velocity of collision. The orienting field also acts to extract $CHCl_2^+$ ions from the collision volume at the beam crossing point through a hole of 4 mm i.d. into a SEM ion detector. The strong field (1.5 kV/cm) ensures the ion collection in the collision volume without any time delay. Subtraction of the background signal due to the direct beam from the signal of total oriented molecular beam enables us to extract the necessary signal only responsible for steric effects. In our previous studies, the total counts of the product ions were used to determine the steric opacity function, in which the relative velocity distribution of collision is averaged out.[13] In the present study, on the other hand, the TOF measurement of the reagent Ar* atoms and CH_3Cl molecules, and the CH_2Cl^+ product ions, made it possible to obtain the steric opacity functions at specified collision energies, alternatively, the collision energy dependence at a specified molecular orientation.

III. Results and Discussion

A. Collision Energy Dependence of Penning Ionization Cross Sections. Figure 2 shows the TOF profiles of $CHCl_2^+$ product ion in the $Ar(^3P_{2,0}) + CHCl_3 \rightarrow Ar + CHCl_2^+ + Cl + e^-$ reaction, where the $CHCl_3$ molecule is oriented in three orientations with respect to the Ar* approach, i.e., CCl_3-end (filled circles), sideways (open squares), and H-end (open triangles) orientation, respectively. The TOF profile of the Ar* primary beam is also shown with small open squares. The experimental error is estimated to be within each representing point. The data points in the energy region between 0.08 and 0.18 eV in Figure 2 were used for the analysis in the present 2D-measurement.

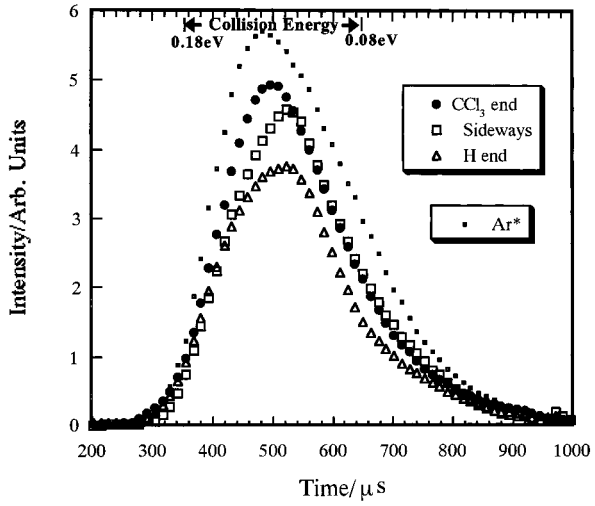

Figure 2. TOF profiles of the product $CHCl_2^+$ ion at three orientations and the Ar* TOF spectrum. (Both arrows) collision energy region of 0.08−0.18 eV used for the analysis.

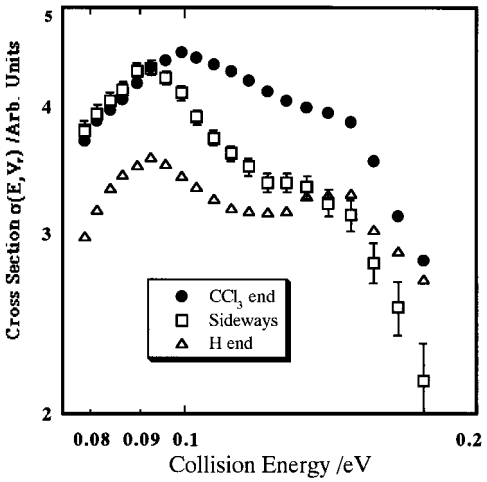

Figure 3. Experimental reaction cross sections as a function of collision energy at three orientation conditions, the CCl_3-end, the H-end, and the sideways orientations.

Figure 3 shows the dependence of the ionization cross section, $\sigma(E,v_r)$ for each of the three orientations in Figure 2. The points are calculated from the experimental points of Figure 2 using the following equation.

$$\sigma(E,v_r) = \frac{R_{CHCl_2^+}(v_r)v_{Ar^*}}{I_{Ar^*}(v_r)n_{CHCl_3}v_r} \quad (1)$$

where $R_{CHCl_2^+}(v_r)$ is the rate of the product $CHCl_2^+$ formation with the dimension of $cm^{-3}\ s^{-1}$ and $I_{Ar^*}(v_r)$ is the flux of Ar* with the dimension of $cm^{-2}\ s^{-1}$ at a specified collision geometry represented by v_r, i.e., the relative velocity vector of the colliding particles $CHCl_3$ and Ar*. v_{Ar^*} is the velocity of Ar*, and n_{CHCl_3} is the number density of the $CHCl_3$ beam. For simplicity, the velocity of $CHCl_3$ can be assumed constant because the velocity spread of the $CHCl_3$ beam is rather narrow as compared with that of Ar*, as shown in the Newton diagram of Figure 1. The pulse shape of the Ar* beam as the shutter function is not taken into account for the convolution of the TOF spectra, because the pulse width is small compared with the energy resolution due to the velocity spread of the $CHCl_3$ beam. Figure 3 reveals that all cross sections commonly increase at the lower collision energy range 0.08−0.1 eV and they start to decrease after that

at higher collision energies, even though the tend of decrease is not monotonic and not similar for each orientation. The curve for sideways orientation (open squares) has a sharper decline than that for either CCl_3-end (filled circles) or H-end (open triangles). These different behaviors among different molecular orientations clearly show the existence of spatial anisotropy in collision energy dependence in chloroform Penning ionization reaction.

B. Velocity-Specified Steric Opacity Functions. In general, the cross section of Penning ionization can be expressed in terms of relative velocity and mutual orientation between two colliders.

$$\sigma(v_r,\cos\gamma) = \sigma(v_r)\, I(v_r,\cos\gamma) \tag{2}$$

where $I(v_r,\cos\gamma)$ is introduced as the "velocity-specified" steric opacity function, and it can be further expanded by Legendre polynomials as follows.[14]

$$I(v_r,\cos\gamma) = \sum S_n(v_r)\, P_n(\cos\gamma) \tag{3}$$

$\sigma(E,v_r)$ of eq 1 is the cross section experimentally obtained, which is weighted by the orientational distribution, $W(E,\cos\theta)$. The latter is also expanded by Legendre polynomials, as shown in[14]

$$W(E,\cos\theta) = \sum C_n(E)\, P_n(\cos\theta) \tag{4}$$

The Legendre moments $C_n(E)$ appearing on the right-hand side of eq 4 can be obtained by simulating the experimental focusing curve, namely the dependence of the beam intensity upon the hexapole rod voltage. Taking into account a so-called "misalignment" between the orientation field vector, **E**, and the relative velocity vector, $\mathbf{V}_r$, $P_n(\mathbf{E}\cdot\mathbf{V}_r)$ is introduced and, finally, the cross section, $\sigma(E,v_r)$ is written

$$\sigma(E,v_r) = \sigma(v_r)\sum S_n(v_r)\,\langle P_n(\mathbf{r}\cdot\mathbf{E})\rangle\, P_n(\mathbf{E}\cdot\mathbf{V}_r) \tag{5}$$

where $S_n(v_r)$ and $\sigma(v_r)$ can be determined by reproducing experimentally obtained cross sections, $\sigma(E,v_r)$. The resultant expansion coefficiencies, $S_1(v_r)$, $S_2(v_r)$ are plotted with the estimated error bars in Figure 4.

In Figure 5, we show 3-D plot of $\sigma(v_r,\cos\gamma)$, the cross section of Penning ionization reaction $Ar(^3P_{2,0}) + CHCl_3 \rightarrow Ar + CHCl_2^+ + Cl + e^-$, as the function of collision energy as well as molecular orientation.

The steric opacity function at a specific collision energy, $I(v_r,\cos\gamma)$ can be obtained by cutting the 3-D plot at corresponding collision energy. Polar representations of $I(v_r,\cos\gamma)$ thus obtained are shown in Figure 6 from 0.081 eV (top curve) to 0.17 eV (bottom curve). The broken vertical line stands for the location of the center of mass of the molecule. The horizontal axis corresponds to the collinear approach of Ar*; the H-end (left) and the CCl_3-end (right). The arrow indicates energy increment. The radial displacement in the polar presentation represents the magnitude of the reaction cross section.

One clearly sees an interesting change of the steric opacity funcrion $I(v_r,\cos\gamma)$ from top to bottom. At low collision energies of 0.081−0.096 eV, it appears that the steric opacity function is very similar to the electron density distribution of the $2a_2$ molecular orbital (MO) for chloroform (see Figure 9). As the collision energy increases, the collinear approach to either the CCl_3-end or the H-end becomes more favorable. Alternatively, the sideways attack becomes unfavorable at higher collision

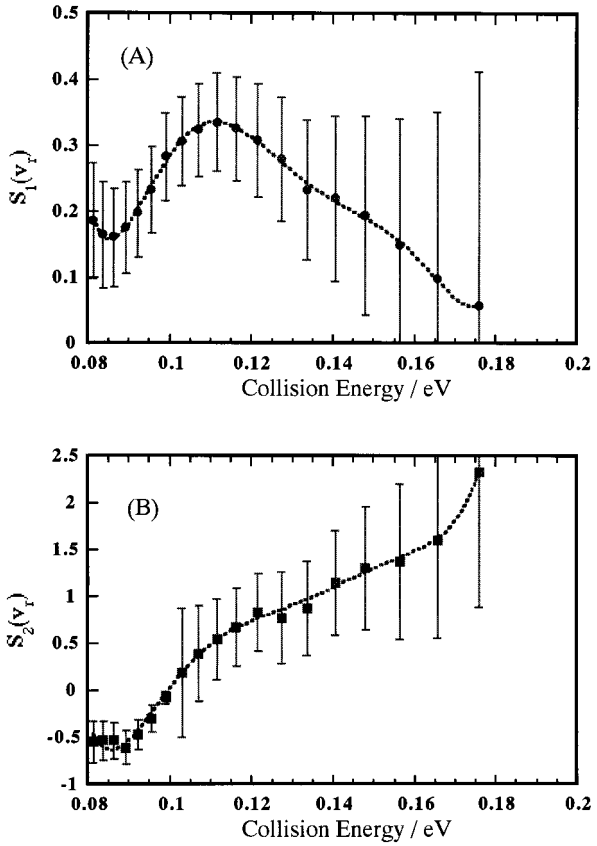

Figure 4. Expansion coefficiencies of the steric opacity function by Legendre polynomials as the function of collision energy: (A) $S_1(v_r)$, (B) $S_2(v_r)$.

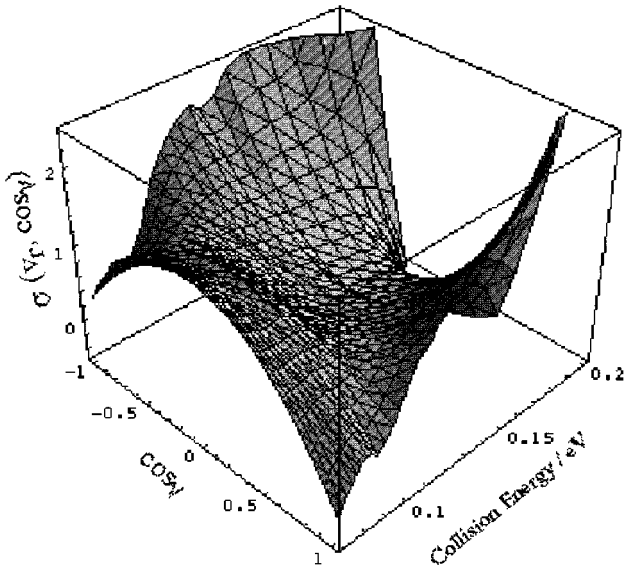

Figure 5. 3-D plot of the reaction cross section, $\sigma(v_r,\cos\gamma)$ as the function of both collision energy and orientational angle.

energy. We shall discuss this aspect more quantitatively in the next section.

The collision energy dependence of the ionization cross section at a specific angle of attack can be obtained by cutting the 3-D plot in Figure 5 at the corresponding orientation. Five representative dependencies are shown in Figure 7. The orientation-specified Penning ionization cross section shows an increase with increasing collision energy at both the CCl_3-end ($\gamma = 20°$) and the H-end ($\gamma = 180°$). While the sideways attack shows a drop with an increase of collision energy. In general, different

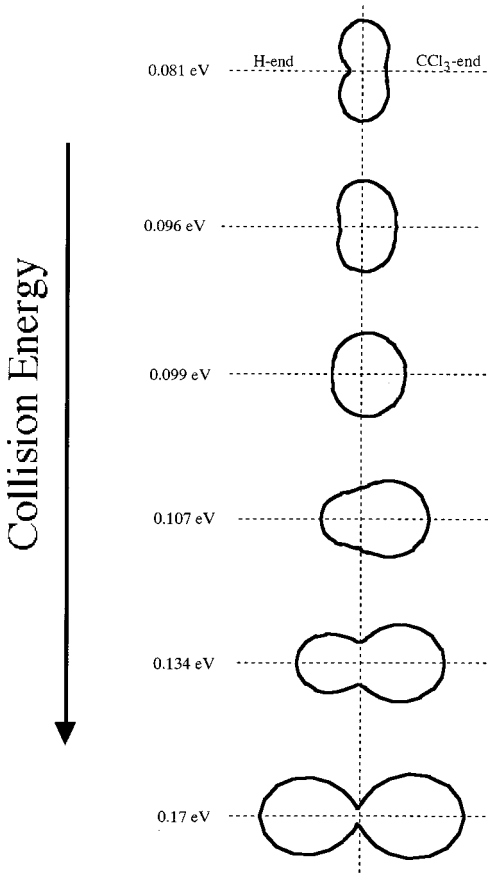

Figure 6. Polar plots of the steric opacity function at the specific collision energy ranging from 0.08 to 0.17 eV.

behavior in collision energy dependence for the ionization cross section can be interpreted due to the difference of interaction potential between the colliding partners.[15] It has been well established that the cross section should show decreasing behavior with collision energy when the collision takes place at an attractive interaction potential, while it should show an increasing behavior for a repulsive potential. If this is the case, it is expected that the collinear collisions must encounter a repulsive wall while sideways collision encounters an attractive potential.

C. Potential Energy Curve of Ar* + $CHCl_3$. To elucidate the above prospect, we have carried out ab initio calculation to obtain the potential energy curves of Ar* + $CHCl_3$ by following a scheme of unrestricted QCISD with 6-31+G(d) basis sets, which takes electron correlation effects into account. The long-range part of interaction between metastable rare-gas atom and molecular interaction is known to resemble the interaction between the corresponding alkaline metal atom and the molecule.[16] A good resemblance of the ground-state K atom to the metastable Ar* atom, Ar(^{3}P), allows us to approximate the Ar* atom by the K atom in the calculation.

In Figure 8, the results of the calculation are presented for five different collision angles of attack. One may easily find that all five orientations mostly exhibit repulsive character, even though some of them exhibit a very shallow well for the H-end, 45°, 135°. As we discussed above, the repulsive behavior on the potential energy curve should be correlated with the increase behavior in the cross section with collision energy. However, the disagreement between the experimental result and the theoretical prediction as for the sideways orientation strongly suggests the necessity of a new factor to be considered for understanding the experimental finding we obtained in the present study.

D. Competition with Other Reaction Channels. It is well-known that de-excitation exit channels other than Penning ionization are likely to open as the mass of rare-gas atom increases.[9] So the Ar* atom could provide more variety of exit channels than He* and Ne*, in opposition to the order of excitation energy of He* and Ne*. Their predominant channel is Penning ionization.

There are at least five ionic states of $CHCl_3$ in the nearby energy region of the entrance channel.[17] They are summarized in Table 1. We must consider also the Rydberg states that converge to $9a_1$, $7e'$, $2e''$, and $6e'$ ionic states within the experimental energy region. At higher collision energy, those Rydberg states tend to cross the Ar* + $CHCl_3$ surface. This level crossing must open up other reaction channels that are competing with Penning ionization. It means that the colliding particles with higher translational energy on the Ar* + $CHCl_3$ potential energy curve could accelerate the chance of coupling with one of the Rydberg states, which subsequently leads to the neutral dissociation of $CHCl_3$*, referred to as the "dark

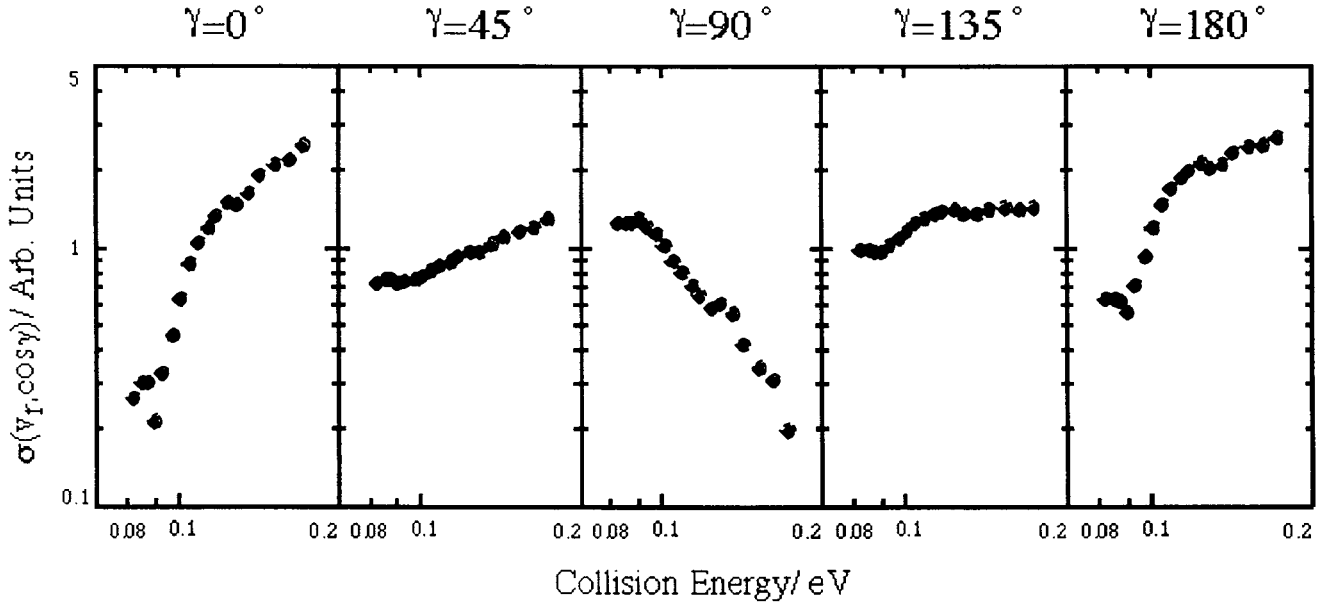

Figure 7. Collision energy dependence of reaction cross sections at the specified orientational angle of 0°, 45°, 90°, 135°, and 180°.

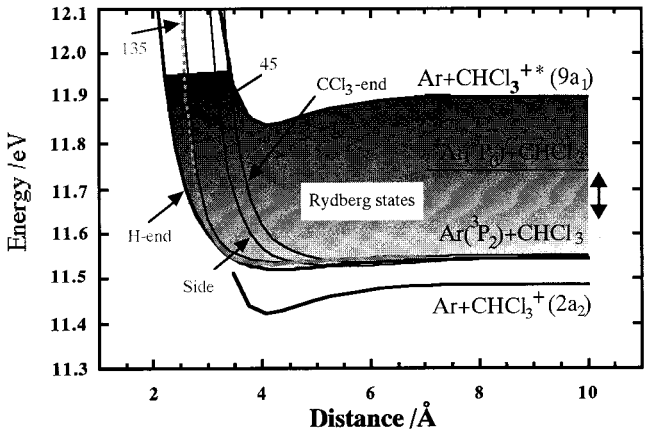

Figure 8. Calculated intermolecular interaction potentials of Ar* + $CHCl_3$ at five different orientation angles. They are determined by ab initio calculation with the unrestricted QCISD with 6-31+G(d) basis sets. Except for the H-end case, the distance is defined as the distance of Ar* approach toward the center of mass of $CHCl_3$. As for the H-end, the distance is defined as the distance of Ar* from the H atom of $CHCl_3$ for avoiding the overlap of the curves. The screened region schematically indicates the Rydberg states that converge to $CHCl_3^+$*($9a_1$). (Both arrows) experimental collision energy region of 0.08−0.18 eV for the $Ar(^3P_2)$ reaction.

TABLE 1: Ionic States in the nearby Energy Regions for a $CHCl_3$ Molecule

orbital	$2a_2$	$9a_1$	7e′	2e″	6e′
ionization energy[a]/eV	11.48	11.91	12.01	12.85	15.99

[a] Data are cited from ref 17.

channel". This dissociation competes with the Penning ionization channel, especially at the sideways orientation. Since very little information is available in the literature about the electronic excitation of $CHCl_3$ in the 11−12 eV energy region, it is difficult to assign which specific Rydberg state is involved in the above-mentioned neutral dissociation. Nonetheless, it is generally recognized that superexcited states and/or Rydberg state molecules are likely to undertake neutral dissociation at relatively high efficiency.[18]

We have therefore calculated some plausible ionic surfaces of Ar + $CHCl_3^+$ in the vicinity of the Ar* + $CHCl_3$ covalent surface using the same method described previously. The result shows that one of them is the $2a_2$ ionic surface located approximately 0.15 eV below the covalent surface, and the second one is the $9a_1$ excited ionic surface located 0.35 eV above the covalent surface.[17] Since the fraction of $Ar(^3P_0)$ is negligible in the metastable atom beam, the CH_2Cl^+ product formation by ejecting an electron from the $2a_2$ orbital is regarded to be the unique process of Penning ionization. Such ionization is initiated if energy transfer occurs between Ar* + $CHCl_3$ and the $2a_2$ ionic surface by ejecting an electron. Penning ionization is regarded to be a major de-excitation process at low collision energy, for it takes place through direct coupling of the entrance surface with the $2a_2$ ionic surface. Thus, the orientation dependence of the ionization must reflect the spatial distribution of electron density of the $2a_2$ molecular orbital, as shown in Figure 9A.

As the collision energy becomes higher, the Rydberg states start to provide a good possibility of the level crossing with the Ar* + $CHCl_3$ surface. The transition probability to the Rydberg states may be expressed as follows:

$$\sigma \propto |\langle \varphi_{\text{final}} | V(R) | \varphi_{\text{initial}} \rangle|^2 \qquad (6)$$

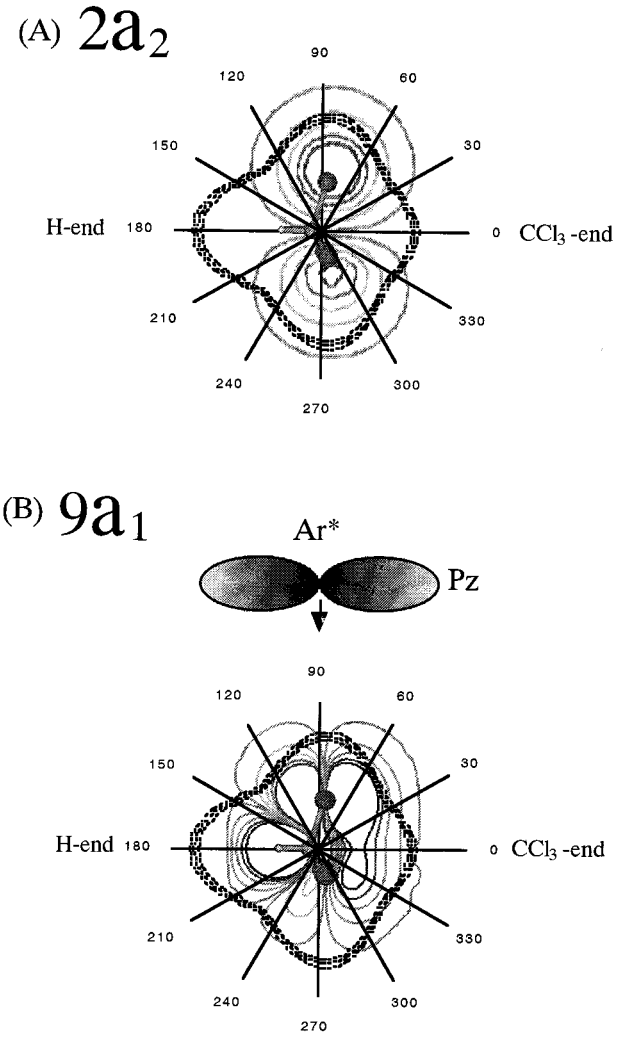

Figure 9. Electron density distributions of (A) HOMO $2a_2$ and (B), $9a_1$ orbital of $CHCl_3$. (Dashed lines) distances of closest approach of Ar* with the translational energy of 0.08−0.18 eV.

where φ_{initial} is the initial state wave function, φ_{final} is the final state wave function, and $V(R)$ is the interaction potential.

As summarized in Table 1, the energies of the molecular orbitals are nearly equal to that of the 3p orbital of $Ar(^3P)$, which is estimated to be 15.76 eV from the ionization potential of Ar. Similarly, the orbital energy of the Rydberg state of CH_3Cl might be nearly equal to that of the 4s orbital of $Ar(^3P)$ which is estimated to be 4.2 eV by using the excitation energy of $Ar(^3P)$, i.e., 11.52 eV. The estimation of the excitation energy strongly suggests that the Rydberg state formation at the curve crossing regions might proceed via the electron exchange mechanism. That is, an electron of the molecule is initially transferred into the vacant inner-shell 3p orbital of $Ar(^3P)$; then an electron in the occupied out-shell 4s orbital of $Ar(^3P)$ is transferred to the Rydberg orbital of CH_3Cl. Within the validity of the electron exchange mechanism for "dark channel" due to Rydberg states formation, the cross section of dark channel is estimated by the exchange type interaction. The initial wave function φ_{initial} is approximated by the product of the molecular orbital MO(1) and the orbital of atom 4s(2). Similarly, the final wave function φ_{final} is represented by the product of the atomic orbital 3p(1) and the Rydberg orbital of the molecule Ryd(2). Therefore, the cross section is expressed

$$\sigma \propto |\langle 3p(1)\ \text{Ryd}(2)\varphi | 1/r_{12} || \text{MO}(1)\ 4s(2)\varphi \rangle|^2 \qquad (7)$$

where 1 and 2 denote the two electrons that exchange and φ represents the core orbitals. The major contribution to σ might be localized in the region where the overlap of the molecular orbital with the 3p hole of Ar(^{3}P) is maximum, because the Rydberg orbital of CH_3Cl might overlap well with the 4s orbital of Ar(^{3}P). This implies that the dark channels are controlled by the overlap integral of the two orbitals, 3p(1) and MO(1), in the electron exchange. A similar stereoselectivity has been revealed in our previous studies on the dissociative energy transfer channels, which also proceeds by the electron exchange mechanism.[19,20] Among the Rydberg states that converge to $9a_1$, 7e′, 2e″, and 6e′ ionic states, the Rydberg states converged to $9a_1$ionic states are expected to have the most important role in the dark channel within the experimental energy region, because the state density of the Rydberg states is steeply increasing as the energy approaches the ionic limit. A closer comparison of the shape of the ionic MO $9a_1$ of $CHCl_3^{+*}$ in Figure 9B obtained by ab initio calculation indicates that the electron density distribution extends sideways toward the molecule. This computational result seems to rationalize the experimental finding that the branching possibility of neutral dissociation is higher at the sideways orientation. Although the detailed theoretical evaluation of the coupling matrix is necessary in order to make clear the proposed mechanism, in a qualitative sense, $3p_z$ orbital of Ar(^{3}P) is expected to efficiently overlap with the exterior electron of the $9a_1$ orbital, despite there being a nodal plane in the sideways orientation. In addition, there are other possibilities to be considered. Considerable reduction of the sideways cross sections may partly connect with the other Rydberg states from the orbitals such as 7e′, 2e″, 6e" orbitals, which also have more electron densities in the sideways direction.

Therefore, we may conclude that the velocity-specified steric opacity function has the potential to represent the dynamical aspect of reaction branching between Penning ionization and neutral dark channels in great detail in the Ar* + $CHCl_3$ reaction.

IV. Conclusions

The Penning ionization cross section of the Ar* + $CHCl_3$ crossed beam reaction is determined as the function of both molecular orientation and relative collision energy using the $CHCl_3$ oriented molecular beam. At lower collision energies, the ionization cross section is found to be most favorable for the sideways orientation. As the collision energy increases, on the other hand, Ar* attacking on the CCl_3-end or the H-end of the target molecule enhances the Penning ionization cross section. This experimental finding implies the competition between Penning ionization and the neutral dissociation at the exit channel, especially at the sideways of the molecule. The ab initio calculation suggested that $CHCl_3$ in a Rydberg state (or states) is likely to correlate to the neutral dissociation channel, which reduces the branching ratio to the Penning ionization channel significantly.

Acknowledgment. The Japanese Ministry of Education, Science, and Culture is gratefully acknowledged for a Grant Aid for Scientific Research (No. 1044174) in support of this work. We thank Professors B. G. Brunetti and F. Vecchiocattivi of Perugia University for valuable discussions and suggestions.

References and Notes

(1) Hotop, H.; Niehaus, A. *Z. Phys.* **1969**, *228*, 68.
(2) Mitsuke, K.; Takami, T.; Ohno, K. *J. Chem. Phys.* **1989**, *91*, 1618.
(3) Ohno, K.; Takami, T.; Mitsuke, K.; Ishida, T. *J. Chem. Phys.* **1991**, *92*, 2675.
(4) Ogawa, T.; Ohno, K. *J. Chem. Phys.* **1999**, *110*, 3733.
(5) Kishimoto, N.; Furuhashi, M.; Ohno, K. *J. Electron. Spectrosc. Relat. Phenom.* **1998**, *88*−*91*, 143.
(6) Dunlavy, D. C.; Siska, P. E. *J. Phys. Chem.* **1996**, *100*, 21.
(7) Brunetti, B.; Candori, P.; De Andres, J.; Pirani, F.; Rosi, M.; Falcinelli, S.; Vecchiocattivi, F. *J. Phys. Chem.* **1997**, *101*, 7505.
(8) BenArfa, M.; Lescop, B.; Cherid, M.; Brunetti, B.; Candori, P.; Malfatti, D.; Vecchiocattivi, F. *Chem. Phys. Lett.* **1999**, *308*, 71.
(9) Jones, M. T.; Dreiling, T. D.; Setser, D. W.; McDonald, R. N. *J. Phys. Chem.* **1985**, *89*, 4501.
(10) Ohoyama, H.; Kawaguchi, H.; Yamato, M.; Kasai, T.; Brunetti, B. G.; Vecchiocattivi, F. *Chem. Phys. Lett.* **1999**, *313*, 484.
(11) Kawaguchi, H.; Ohoyama, H.; Kasai, T. *Chem. Lett* **1998,** 629.
(12) Imura, K.; Midorikawa, R.; Kasai, T.; Ohoyama, H.; Che, D.-C. *Chem. Lett*. **1996**, 299.
(13) Yamato, M.; Wu, V. W.-K.; Okada, S.; Ohoyama, H.; Kasai, T. *J. Chem. Phys.* **2000**, *113*, 6673.
(14) Stolte, S.; Chakravorty, K. K.; Bernstein, R. B.; Parker, D. H. *Chem. Phys.* **1982**, *71*, 353.
(15) Aguilar, A.; Brunetti, B. G.; Gonzalez, M.; Vecchiocattivi, F. *Chem. Phys.* **1990**, *145*, 211.
(16) Fraites, J. L.; Winicur, D. H. *Mol. Phys.* **1978**, *35*, 927.
(17) Kimura, K.; Katsumata, S.; Achiba, Y.; Yamazaki, T.; Iwata, S. *Handbook of He I Photoelectron Spectra of Fundamental Organic Molecules*; Japan Scientific: Tokyo, 1981.
(18) Hatano, Y. *Phys. Rep.* **1999**, *313*, 109 and references therein.
(19) Ohoyama, H.; Kasai, T.; Ohashi, K.; Kuwata, K. *Chem. Phys.* **1992**, *165*, 155.
(20) Takahashi, H.; Ohoyama, H.; Kasai, T.; Nakano, M.; Yamaguchi, K. *J. Phys. Chem.* **1995**, *99*, 13600.